An overview on the use of graphene-based membranes for membrane distillation

Nurul Syazana Fuzil[a], Nur Hidayati Othman[a,*], Nur Hashimah Alias[a], Muhammad Shafiq Mat Shayuti[a], Munawar Zaman Shahruddin[a], Fauziah Marpani[a], Woei Jye Lau[b], Ahmad Fauzi Ismail[b], Mohd Hafiz Dzarfan Othman[b], Tutuk Djoko Kusworo[c], Mohammad Mahdi A. Shirazi[d]

[a]*Catalysis for Sustainable Water and Energy Nexus Research Group, School of Chemical Engineering, College of Engineering, Universiti Teknologi MARA, 40450 Shah Alam, Selangor, Malaysia, emails: nurhidayati0955@uitm.edu.my (N.H. Othman), syazanafuzil@gmail.com (N.S. Fuzil), nurhashimah@uitm.edu.my (N.H. Alias), mshafiq5779@uitm.edu.my (M.S.M. Shayuti), munawar_zaman@.uitm.edu.my (M.Z. Shahruddin), fauziah176@uitm.edu.my (F. Marpani)*
[b]*Advanced Membrane Technology Research Centre (AMTEC), Universiti Teknologi Malaysia, 81310 Skudai, Johor, Malaysia, emails: wjlau@petroleum.utm.my (W.J. Lau), afauzi@utm.my (A.F. Ismail), hafiz@petroleum.utm.my (M.H.D Othman)*
[c]*Department of Chemical Engineering, Faculty of Engineering, Diponegoro University, Semarang, 50275, Indonesia, email: tdkusworo@che.undip.ac.id (T.D. Kusworo)*
[d]*Chemical Engineering Department, Faculty of Engineering, University of Kashan, 8731753153 Kashan, Iran, email: mmahdiashirazi@gmail.com (M.M.A. Shirazi)*

ABSTRACT

Recently, a thermally-driven membrane process known as membrane distillation (MD) has emerged as an alternative to the high-pressure membrane process for contaminants removal from water. The driving force for MD is a vapor pressure gradient produced by a temperature differential across a hydrophobic porous membrane, which results in the transfer of water vapor from hot to cold side. However, the feasibility of MD for industry adoption is hampered by several issues such as temperature polarisation effects, low permeate flux, membrane wetting, and fouling. The membrane properties are known to have a significant role in controlling the final performances of MD. This review first looks into the feature of ideal MD membrane properties. Then, the use of graphene-based materials for the development of high performances MD membrane is discussed. Besides enhancing the water permeability and selectivity of MD, the incorporation of graphene offers additional properties such as anti-fouling, antibacterial, and photodegradation. The future direction of using graphene-based photothermal material in MD for heat generation under solar irradiation is also reviewed. It is found that the localised heating at membrane surfaces by photothermal material can minimise temperature polarisation effects and subsequently enhance the driving force for effective vapour transport. Thus, a more energy-efficient MD system can be developed.

Keywords: Membrane; Graphene; Membrane distillation, Photothermal; Desalination; Water purification

1. Introduction

Water stress or scarcity occurred when the demand for clean water exceeded the water resources and supply. Many countries have been facing water stress and water shortage problems over the past decades due to several factors such as population growth, increase in water pollution, and climate change [1]. Keeping water consumption at a sustainable level is getting more difficult in the near future. Thus, water treatment technologies improvement is vital to curb this problem [2]. Desalination is the process of removing dissolved salts from various sources such as seawater, brackish waters, or highly mineralised groundwaters. It has been considered as the main source for producing clean water for domestic and industrial use [3]. Today, a pressure-driven reverse osmosis (RO) membrane is one of the leading technologies for desalination due to its high separation capabilities, compact design, simple operation, and more energy-efficient than vaporisation and distillation processes. RO separates contaminants using high pressure to force the contaminated water through a semipermeable membrane. The solute is retained on the pressurised side of the membrane, and pure water is allowed to pass to the other side (Fig. 1a). However, the RO process faces challenges such as fouling, high energy consumption due to the need for very high-pressure pumping, and brine disposal problems due to the limited recovery of water [4]. As a result, more sustainable and innovative practice of membrane technology is needed [5,6].

In this context, membrane distillation (MD) has emerged as an alternative membrane-based process due to its ability to distilled water at low temperatures than conventional distillation, [7] while operating at a lower pressure than RO [7]. MD is a non-isothermal process where a hot feed side and a cold permeate side are separated by a hydrophobic microporous membrane [8] (Fig. 1b). The driving force of MD is the vapour pressure difference caused by temperature difference across the membrane [9]. In general, the feed water is heated to increase its vapor pressure, which generates the difference between the partial pressure at both sides of the membrane. The water evaporates at the hot membrane surface, which is then transported to the membrane pores and condenses at the cold permeates side to produce freshwater (Fig. 1b) [10]. Many works have found that MD is not only suitable for high salinity wastewater, but also shows great potential for various wastewater treatment from pharmaceutical, food and beverages, and biomedical industries.

MD typically has lower capital costs than the conventional distillation process. In addition, it requires low-temperature input, allowing the use of low-grade and inexpensive heat sources. Another advantage of MD is that the fouling is less severe than RO. However, the commercialisation of MD is still hindered by technical challenges such as temperature polarisation (TP), concentration polarisation, heat losses, and pore wetting [11]. Temperature polarisation is caused by the temperature gradient between bulk feed and membrane surface at the liquid/vapor interface. The vaporisation decreases the liquid bulk temperature while increasing the vapor temperature. This leads to a reduction of temperature difference, leading to permeate flux decline. Concentration polarisation can reduce the transmembrane vapor pressure difference, and it is caused by the accumulation of solutes adjacent to the feed side of the membrane.

2. Configurations of membrane distillation

There are four main MD configurations where the difference is the water collection method or condensation. The simplest MD configuration is direct contact membrane distillation (DCMD). In this configuration, the hot feed solution and cool permeate flow in counter-current (Fig. 2). The vapour is transported through the membrane due to
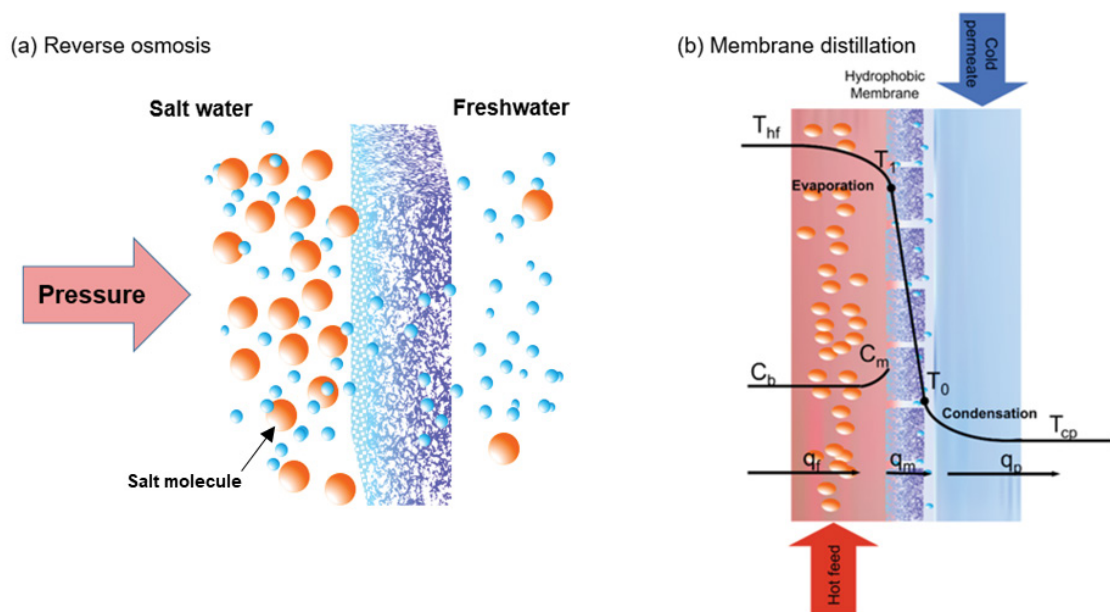

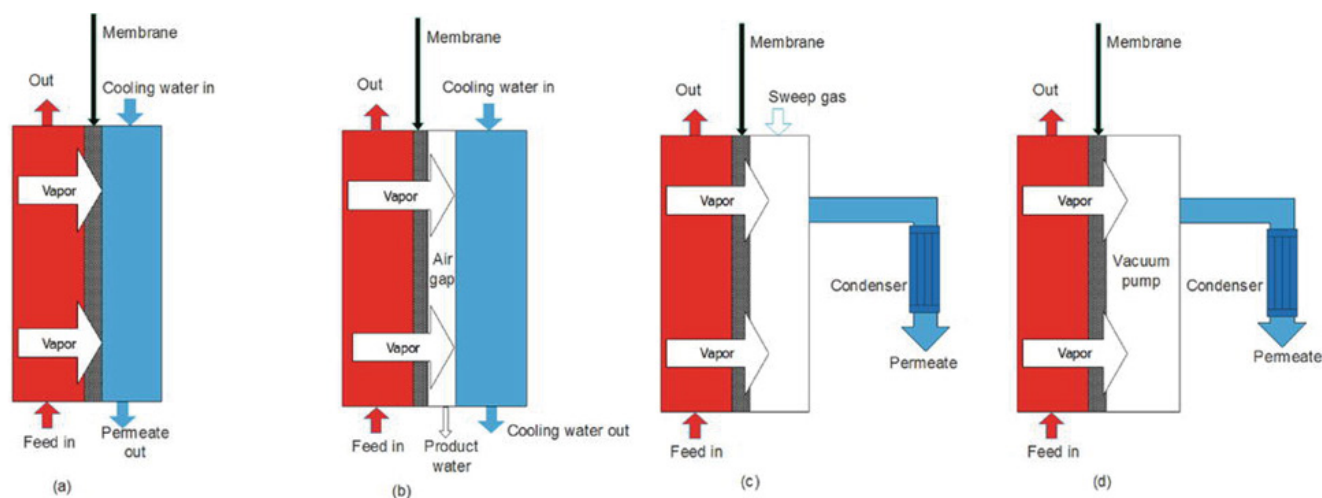Fig. 1. Schematic diagram of (a) RO and (b) MD process [10].

Fig. 2. Schematic diagram of membrane distillation configuration: DCMD, AGMD, SGMD, and VMD processes [16].

temperature-induced vapour pressure gradient. The advantage of this configuration is that it has a simple design and is easy to operate, making it suitable for laboratories-scale investigation. However, DCMD typically exhibits poor wettability resistance and requires a heat exchanger to recover the heat [12]. In the air-gap membrane distillation (AGMD), an air-filled cavity is interposed between a porous hydrophobic membrane and the condensation surface. It allows the internal recovery of heat and provides high thermal insulation between channels to minimise overall heat transfer, making AGMD is the most energy-efficient configuration [12].

Vacuum membrane distillation (VMD) utilises vacuum at permeate side of the membrane for continuous vapour removal from the vacuum chamber. The advantage of this configuration is that it permits high flux and reduces the probability of the membrane pore being blocked. However, it is a complex configuration [13]. Sweep gas membrane distillation (SGMD) uses cold, inert gas, such as air or nitrogen, at the permeate side of the membrane to sweep and carry the evaporated molecules outside the membrane module for condensation. SGMD has higher evaporation efficiency than DCMD and greater permeate flux than AGMD, due to the low conductive heat loss and the reduced mass transfer resistance, respectively [14]. However, the application of SGMD is limited as a result of its high sweeping gas cost and difficulty in heat recovery [15].

3. Membrane properties for membrane distillation application

One of the building blocks in developing a highly efficient MD system is the membrane itself. MD uses a hydrophobic microporous membrane to prevent the transport of aqueous feed through the micropores and only allows water vapour transport due to the difference of partial pressures established across the membrane. Therefore, it is vital to understand the properties of the required membrane to maximise the overall efficiency of the MD system. Among those properties are liquid entry pressure (LEP), membrane thickness, porosity, pore size, water contact angle (hydrophobicity), and thermal conductivity.

3.1. Liquid entry pressure

LEP indicates the membrane resistance toward the pore wetting phenomenon when the feed solution directly contacts the membrane surface. In MD process, LEP is defined as the minimum transmembrane pressure required for the feed solution to overcome the hydrophobic forces and penetrate the membrane pores. It is vital to ensure that the pressure applied does not exceed the LEP so that the liquid feed cannot penetrate the membrane pores. The high LEP indicates better membrane wetting prevention. LEP is highly dependent on the shape and size of the pores, the liquid surface tension, and the membrane hydrophobicity (>90°). Cantor–Laplace equation is used to provide the relationship between the membrane's largest allowable pore size and operating conditions, as shown in Eq. (1):

$$LEP = P_{liquid} - P_{vapor} = \frac{-2\beta\gamma_L \cos\theta}{r_{max}} \tag{1}$$

In order to achieve a high LEP value, the surface contact angle (θ), surface tension (γ_L), and geometric coefficient (β) should be high, while the maximum pore radius (r_{max}) value should be as low as possible [17]. Thus, high LEP can be achieved using membrane material with high hydrophobicity and small maximum pore size. However, when the maximum pore size decreases, the membrane permeability decreases due to low mean pore size of the membrane.

A typical setup for an LEP system analysis is shown in Fig. 3 [17]. Kebria et al. [18] analysed the LEP of membrane using a dead-end LEP cell, where the pressure was increased by 0.2 bar for every 5 min period. At the first appearance of a water drop, the pressure value is known as LEP. Smaller mean surface pore size typically delivers higher LEP [18]. Ghim et al. [19] produced a membrane with 122 kPa of LEP, while Said et al. [20] fabricated a
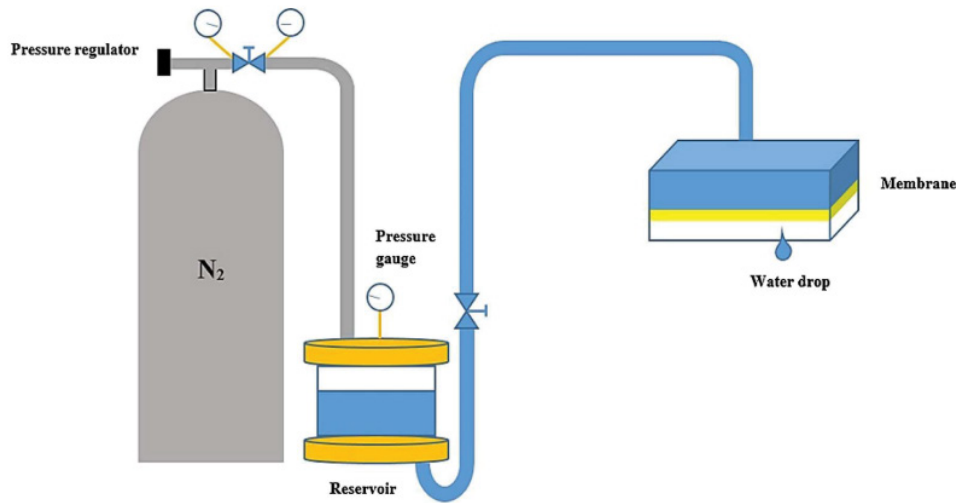
Fig. 3. Schematic diagram LEP system setup [17].

membrane with 317.2 kPa LEP value. These high LEP values can inhibit direct liquid mixing between the feed water and the permeate during MD operation.

3.2. Membrane thickness

Membrane thickness can significantly influence permeate flux. The membrane thickness and membrane permeate flux are inversely related to each other. As the thickness of the membrane decreases, the permeate flux enhances due to the reduction in mass transfer resistance [21,22]. However, if the membrane is too thin, the vapour flux could also decrease because of the conduction losses. Thus, there is a trade-off between the advantage (higher permeate flux) and the disadvantage (higher heat loss) when a thinner membrane is used. Swaminathan et al. [23] stated that an optimum membrane thickness depends on the feed concentration, where high salinity feed concentration typically requires thicker membranes to withstand the highly concentrated feed. Tai et al. [24] reported that the membrane thickness for MD is optimum at a range between 30–60 μm, and for AGMD configuration, the membrane thickness has a negligible effect on the performance due to the dominant mass transfer resistance in the configuration caused by the air gap.

3.3. Membrane porosity and tortuosity

Membrane porosity indicates the void volume fraction of the membrane. It is calculated based on the ratio of the pore volume over the total membrane volume. The porosity of membranes should be as high as possible to eliminate the wetting phenomenon and enhance the permeation flux. Higher porosity membranes also indicate larger evaporation surface area. The membrane porosity is calculated using the gravimetric method (Eq. 2) [25] by applying wetting liquid such as 2-propanol [26], octanol [27], or n-butanol [28].

$$\varepsilon = \frac{\left(w_w - w_d\right)/\rho_i}{\dfrac{\left(w_w - w_d\right)}{\rho_i} + \dfrac{w_d}{\rho_p}} \times 100\% \tag{2}$$

where ε is the membrane void volume fraction, w_d and w_w are the weight of the membrane before and after immersing in wetting liquid, respectively, ρ_i is the density of the wetting liquid, ρ_p is the polymer density, and V_d is the dry membrane volume [28]. For flat sheet membrane, Eq. (2) is revised into:

$$\varepsilon = \frac{\left(w_w - w_d\right)/\rho_i}{Al} \times 100\% \tag{3}$$

where A is the membrane area, and l is the membrane thickness. A membrane with typical porosity of 60%–85% is commonly used in the MD system [29].

According to Mortaheb et al. [26], a dope solution with high amount of polymer typically produces membrane with low porosity due to the highly viscous dope solution. The viscous dope solution will form a dense top layer during the spinning or casting process due to the slow phase inversion between the solvent in the dope solution and the non-solvent in the coagulation bath. Shirazi et al. [30] proposed the use of the electrospinning method to produce a membrane with high porosity (>90%), where nanofiber that has open-ended pores with interconnected three-dimensional (3D) structures can be obtained.

Membrane tortuosity is the deviation of the pore structure from the cylindrical shape to the membrane surface, as the membrane pores are full of twists and turns. Low membrane tortuosity is desirable in order to achieve a higher permeate flux because diffusing vapour molecules must pass along the tortuous paths to reach the other side of the membrane [30]. An ideal membrane tortuosity in MD application is close to zero and several studies have

investigated the use of nanoparticles, such as graphene oxide (GO) [31].

3.4. Mean pore size and pore size distribution

In MD, large mean pore size and narrow pore size distribution are favourable. A high mean pore size would result in a higher permeate flux, while a more limited pore size distribution indicates the uniformity of the membrane structure and the absence of agglomeration [32]. In contrast, a small mean membrane pore size would lead to a higher LEP value. Therefore, the membrane pore size should be controlled appropriately to be in an optimum range to ensure sufficient permeate flux and LEP. The pore size is mainly dependent on the membrane fabrication process, particularly polymer solution composition, the solvent/non-solvent system, membrane fabrication parameters, and ambient conditions [33]. Eykens et al. [34] stated that an ideal membrane for MD should be fabricated with pore diameters ranging between 0.05 to 1 mm. Fang et al. [35] used a thermally induced phase separation (TIPS) to form membranes with better mechanical strength, more uniform structure, and narrower pore size distribution as compared to nonsolvent-induced phase separation (NIPS).

3.5. Membrane hydrophobicity

Membrane for MD should have higher hydrophobicity, as it can prevent membrane pore wetting phenomenon and ensure that only vapour passes through the membrane. This membrane hydrophobicity can be determined using contact angle analysis. Since water is the major component in the MD feed solution, the water contact angle (WCA) is measured for determining the surface's tendency to water droplets. The WCA analysis is carried out by dropping a drop of water on the membrane surface and the angle between the water droplet and membrane surface is assessed [36]. Membranes are considered hydrophobic when their WCA is more than 90° and superhydrophobic when the WCA is more than 150°. The hydrophobicity can be enhanced when the membrane has low surface energy and high surface roughness [37]. Many studies have been carried out to enhance membrane hydrophobicity by modifying the membrane surface energy and surface roughness [37–39].

3.6. Thermal conductivity

MD membrane should have as low thermal conductivity as possible to reduce heat conduction and minimise heat loss during the separation process. Based on Eq. (4), it can be seen that the thermal conductivity is significantly affected by the membrane porosity.

$$\lambda = \lambda_v \varepsilon + \lambda_m \left(1 - \varepsilon\right) \tag{4}$$

where λ is the thermal conductivity of the membrane in W m⁻¹ K⁻¹, ε is the porosity of the membrane, while λ_v and λ_m are the thermal conductivity values of the voids and the membrane materials, respectively [40]. From the equation, it can be seen that a membrane with higher porosity has lower thermal conductivity.

3.7. Challenges in membrane development for MD

One of the major drawbacks associated with MD is temperature polarisation. It is a phenomenon where the hot side membrane surface temperature is lower than that of the hot side main body due to water evaporation, while the cold side membrane surface temperature is higher than that of the cold side main body. This reduces the effective driving force of temperature difference on both sides of the membrane and further reduces the heat transfer rate, which ultimately offset the MD performances. Membrane fouling refers to the phenomenon where contaminants start to deposit on the membrane surface or in membrane pores. The deposit on the membrane surface is one of the significant operating problems which can decrease the permeation flux with operating time. Other barrier for MD is the membrane wetting, where the membrane progressively loses hydrophobicity due to the adsorption of surface-active compounds such as surfactants and oils. The hydrophobic tails of these compounds can attach onto the hydrophobic membrane pore surface, leaving the hydrophilic head exposed and eventually reducing the surface tension. This renders the membrane pores hydrophilic, allowing the feed solution to leak through and contaminate the permeate. For future commercialisation of MD, stable performance over a long term operation is the most crucial aspect.

In order to overcome the challenges, several innovative approaches have been investigated, particularly on the incorporation of nanoparticles (NPs) in the membranes. These NPs are usually dispersed in the polymer membrane matrix or can be coated or grafted on the membrane surface with further functionalisation to enhance the adhesion of NPs. These NPs have remarkable high specific surface area properties, high strength, tuneable hydrophobicity, enhanced vapour transport, and high thermal and electrical conductivities. Many works have observed that the incorporation of nanomaterials such as ZnO [41], MXene [42], and SiO_2 [43] in membranes can significantly enhance water permeability, separation efficiency, and mechanical strength while minimising membrane fouling. Recently, the use of 2D-based nanomaterials for membrane fabrication particularly graphene-based materials has gained great attention due to its potential to produce ultrathin membranes (with a tunable pore size acting as a molecular sieve) with superior performance in terms of permeability and selectivity [44].

4. Graphene

Graphene has a hexagonal honeycomb lattice structure in a two-dimensional (2D) sheet with a thickness of an atom that has sp² bonded length of 0.142 nm [45], a large specific surface area of 2,630 m² g⁻¹ [46], high thermal conductivity at 5,300 W m K⁻¹, and electrical conductivity at 2,000 S cm⁻¹ [47]. Graphene is a breakthrough in material studies because it is very thin yet stronger than steel. In photothermal application, graphene can absorb a wide range of the solar spectrum, with the excited electrons fall to their ground state and release lots of heat compared to other types of material [48]. In addition to the wide range of solar absorption, graphene has higher heat stability from the sunlight due to its 2D shape. The structure of graphene can also be easily

modified due to the number of functional groups available to give higher efficiency of heat absorption, making it a feasible membrane for solar distillation or filtration [49].

4.1. Synthesis of graphene

Graphene can be produced in several ways, where high-quality graphene is typically obtained via chemical vapour deposition (CVD). However, the cheapest and easiest route to mass-produce graphene is by converting graphite into graphene oxide (GO), and its reduction thereof known as reduced graphene oxide (rGO) [50]. The graphite needs to undergo an oxidation process to form graphene oxide, followed by a reduction process (Fig. 4). The above-mentioned reduction can be carried out via chemical, thermal, and electrochemical routes.

4.2. Incorporation of graphene into membranes

Nanocomposite membranes are made up by dispersing nanosized fillers throughout the polymeric matrix. This can significantly improve the membrane properties (porosity, tortuosity, contact angle, etc.), adding unique functionalities such as antibacterial, photocatalytic, adsorptive, and oxidative properties, which simultaneously enhance the membrane performance (flux, rejection, mechanical strength, anti-fouling, permeability, and selectivity) [52–54]. The primary objective of adding graphene into MD membrane is to reduce the wetting of the membrane by increasing the hydrophobicity of the membrane. In addition, graphene is added to improve mass transfer rates by increasing the flux

Fig. 4. Schematic diagram of GO and rGO synthesis [51].

without significantly affecting the rejection rate, leading to a highly efficient system at a lower cost.

Based on the location of NPs embedment, different types of nanocomposite membranes can be manufactured, including conventional mix-matrix nanocomposite, thin-film nanocomposite, thin-film composite with nanocomposite substrate, and surface located nanocomposite [55]. Generally, there are two common techniques used to incorporate graphene into the membrane: (i) conventional nanocomposite or mixed matrix membrane (MMM) where graphene is blended during the dope solution preparation, or (ii) the graphene is used as a coating layer to modify the membrane surface (Fig. 5).

4.2.1. Mixed matrix membrane

In MMM, graphene is added directly into the dope solution containing polymer and solvent before being cast to form a flat sheet membrane (Fig. 6). Besides casting the MMM on a glass plate [41], an electrospinning process can also be used to produce a modified nanofiber MMM [56]. In recent research, Alammar et al. [55] mixed GO, rGO and polybenzimidazole (PBI) into a dope solution before casting to produce MMM and then dip-coating into polydopamine (PDA) solution to enhance the anti-fouling properties. This modification with GO increased the mechanical strength of the membrane with superior oil removal efficiency up to 99.9% and permeate flux about 91.3 ± 3.4 L m^{-2} h^{-1} bar^{-1}.

Baig et al. [61] fabricated a novel composite of PES/PVDF (polyvinylidene fluoride) blended with graphene nanoplatelets (GNPs) via electrospinning process. By adding 2 wt.% GNP into the PES/PVDF blend, the water contact angle (WCA) increased to 132.3° ± 0.8°, making it suitable for MD. The membrane showed a high flux of about 19.35 kg m^{-2} h^{-1}, higher than pure PVDF and PVDF/GNPs composite membranes [57]. Camacho et al. [31] prepared a graphene oxide-polysulfone (GO-PSF) membrane with 0.25–2.0 wt.% GO content in the membranes for membrane distillation application. The addition of GO into the membrane increased the membrane hydrophobicity with WCA of 83° compared to the pristine membrane (WCA 73°), yielding the highest salt rejection of 99.85% and average flux of 20.8 L m^{-2} h^{-1}. The presence of GO in GO-PSF membrane showed good porosity, pore size, and hydrophobic properties for separation. Kadhim et al. [58] modified polyethersulfone (PES) by blending the membrane with GO nanoparticle (NPs) for dye removal application. The modified membrane displayed a high dye rejection efficiency of 99% for very hazardous dyes (Acid Black and Rose Bengal).
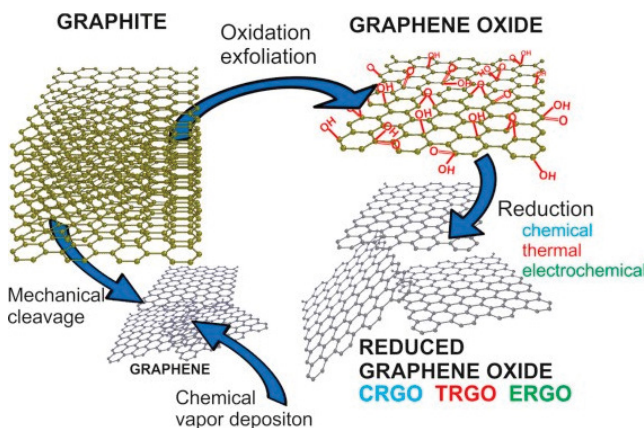

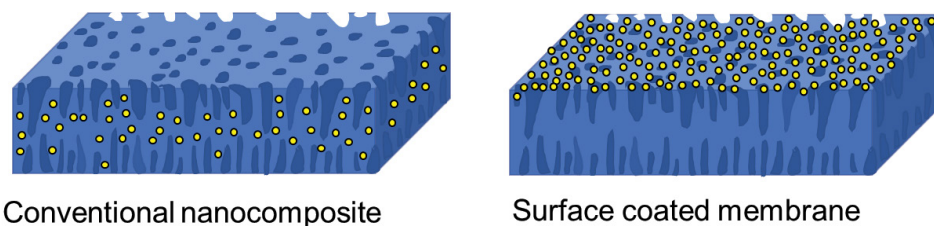Conventional nanocomposite   Surface coated membrane
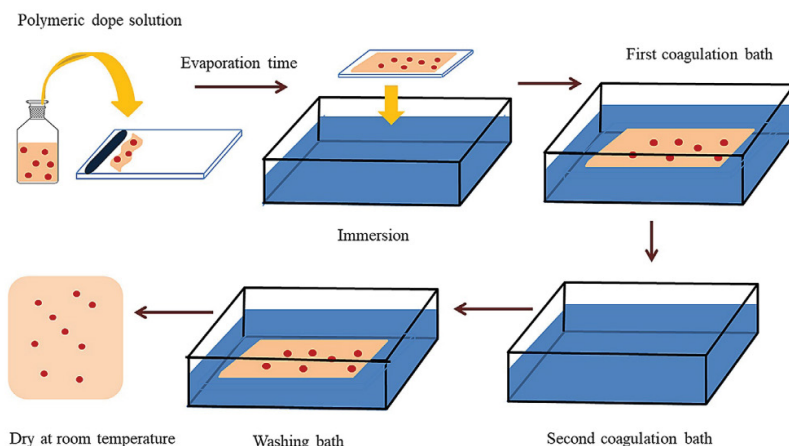
Fig. 5. Incorporation of graphene into membranes.

Fig. 6. Schematic diagram of MMM casting [52].
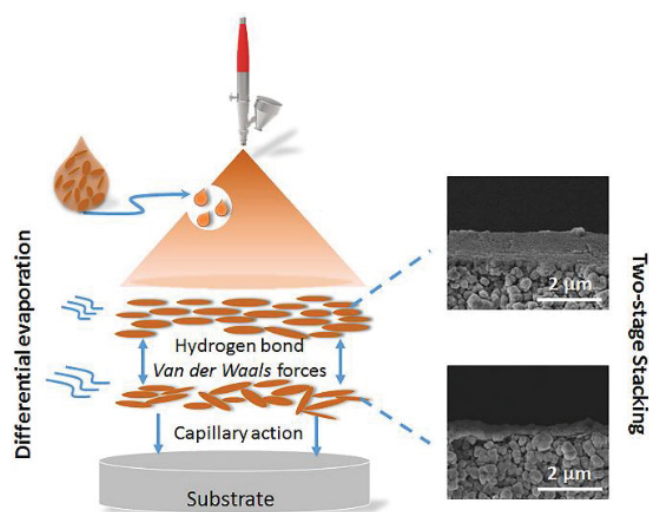
Fig. 7. Schematic diagram of GO spraying onto the substrate [65].

Fig. 8. Polymerisation of GO and GO-TiO$_2$ with polyamide layer [61].

4.2.2. Coating

Graphene can also be coated or deposited onto a membrane surface to modify the surface properties, making it more hydrophobic or less wetting. The coating process can be carried out using several methods such as thermal spraying [59,60], polymerisation [61], and filtration [62–64]. Guan et al. [65] fabricated a GO membrane by spraying the GO suspension onto the heated alumina substrate, as shown in Fig. 7. The spraying process is commonly carried out multiple times to obtain a uniform coating. As the thickness of the GO increases, the permeate flux through the GO layer might decrease due to enhanced mass transfer.

Baig et al. [61] polymerised GO and GO-TiO$_2$ (GT) with the polyamide layer (Fig. 8). The result shows that both nanofillers were firmly attached to the polyamide layer via hydrogen and covalent bonds. GT membranes have higher surface roughness and better hydrophilicity. GT membranes also have more carboxyl groups and a lesser degree of cross-linking due to the interference with the interfacial polymerisation reaction. Thus, GT membranes deliver
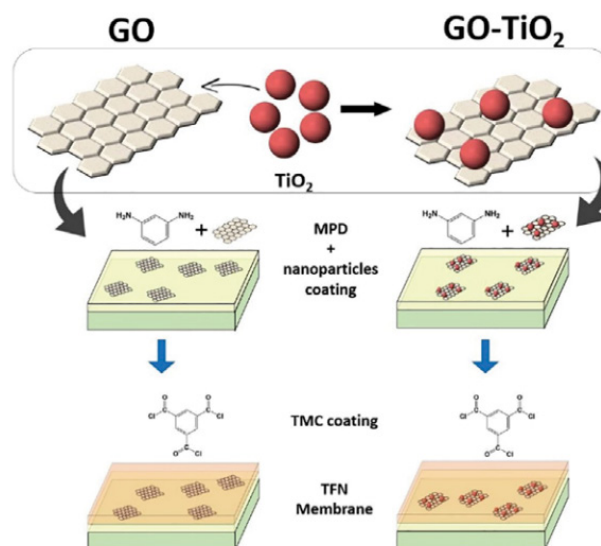
higher permeance (2820 GPU) and water vapour/nitrogen selectivity.

Hassanpour et al. [63] incorporated GO/ZnO composite membrane via filtration on the polyethersulfone (PES) membrane substrate. In order to lower the interlayer spacing between ZnO and GO composite membrane and make the modified membrane more stable, the membrane was treated with UV light for 5–300 min. This modification with GO/ZnO composite increased the membrane water permeability (five times higher than GO membrane), physical compaction, and anti-fouling properties. Furthermore, this membrane could inhibit *Escherichia coli* B bacterial growth. Zhang et al. [64] also applied the filtration technique to fabricate GO/halloysite nanotube (HNT) composite membrane for oil/water separation application. The GO/HNTs composite membrane had a water flux of 1,470 L m^{-2} h^{-1} with GO/HNTs content ratio of 1/3 and high rejection of 99.5%. The membrane also diplayed reusability, as the high-water flux remained after ten times of repeated use.

5. Application of graphene-modified membrane in membrane distillation

The incorporation of graphene into various types of membrane materials, such as polysulfone (PSF), polypropylene (PP), or polytetrafluoroethylene (PTFE) have been widely investigated. Graphene can enhance membrane anti-fouling properties and mechanical stability for long-term application. As such, the graphene-modified membranes were used in MD applications for desalination and oily wastewater treatment.

5.1. Desalination

Recently, the use of graphene-based MD for desalination process has attracted significant attention. The feed concentration used for desalination is typically varied between 3,500 and 34,000 ppm. Zahirifar et al. [21] prepared a layer of octadecylamine functionalised graphene oxide (GO-ODA) coated on the surface of the PVDF membrane. The modified membranes showed a better performance than the bare membrane in terms of hydrophobicity with WCA of 146°, water flux of 16.7 kg m^{-2} h^{-1}, and salt rejection of 98.3%. This was because the GO-ODA coating layer formed interconnected nanochannels with a high surface area for high NaCl rejection and fast water flow. Moreover, during the 5-d continuous desalination process, the modified membrane exhibited a stable performance, showing its durability for long-term use. Bhadra et al. [66] discovered that graphene oxide in the membrane significantly increased the salt rejection efficiency and water flux due to the presence of polar

functional groups in graphene oxide. Although there was a decrease in contact angle, it was insignificant. Mortaheb et al. [26] optimised the hybrid PVDF/graphene membrane prepared via the phase inversion method and discovered that by increasing ethanol concentration in the coagulation bath and graphene content up to 0.5 wt.% in the dope solution, the contact angle and permeation flux of the membrane increased. However, adding more graphene could make the surface pore size low, resulting in a dense membrane surface. The optimum membrane yielded a high permeation flux of 3.54 kg m^{-2} h^{-1} and a salt rejection of 99.88%.

The use of a graphene-modified membrane in MD for desalination application is summarised in Table 1. Based on the table, graphene has gained much attention in enhancing the membrane for MD application as it can help improve the salt rejection efficiency up to more than 99.7% can be achieved. However, the graphene-based material particularly GO has also been modified with hydrophobic modifiers such as octadecylamine (ODA) and 1H,1H,2H,2H-perfl uorooctyltriethoxysilane (FTES) to increase the membrane contact angle and permeate flux as GO is typically rich with hydroxyl group.

Recent studies have incorporated graphene with other potential materials to maximise the potential possessed by graphene. Bhadra et al. [66] sonicated GO with PVDF while polytetrafluoroethylene (PTFE) was used as the membrane support, aiming to repel saltwater cluster. The results show that the membrane had a high thermal conductivity of 5,000 W m^{-1} K^{-1}. The membrane distillation flux achieved was 97 kg m^{-2} h^{-1} at 80°C. It was unaffected by salt

Table 1
Graphene-modified membrane distillation for desalination

Modifier	Membrane	Incorporation	Water contact angle (°)	Permeate flux (kg m^{-2} h^{-1})	Rejection (%)	References
ODA	GO-ODA modified on PVDF membrane (60.5% porosity)	MMM	146.0	16.7	98.3	[21]
PVDF	GO modified on PTFE membrane with PVDF as a binder	MMM	90.6°	97.0	100.0	[66]
–	PVDF/graphene membrane (74.0% porosity)	MMM	92.0	11.3	99.9	[26]
ODA, LiCl	Electrospun polyvinylidene fluoride-*co*-hexafluoropropylene (PVDF-HFP) and ODA-rGO membrane (0.24 μm mean pore size,70.5% porosity)	MMM	146.0	21.1	99.9	[67]
–	GO-polysulfone (GO-PSF) membranes (30.3% porosity, 89 nm mean pore size)	MMM	78.0	20.8 L m^{-2} h^{-1}	99.8	[31]
FTES	FTES functionalised GO nanosheet incorporated into PVDF membrane (96.3% porosity, 186.1 nm average pore size)	MMM	140.5	36.4	99.9	[68]
PDA	PVDF/PDA/GO composite membrane (150 μm thickness)	Coating via evaporation-assisted technique	80.0	17.8	99.9	[69]
–	Electrospun rGO/PVDF membrane (175.7 μm thickness)	MMM	124.5	29.9 L m^{-2} h^{-1}	99.7	[56]

MMM – mixed matrix membrane.

concentration as high as 34,000 ppm, as shown in Fig. 10, and obtained close to 100% salt rejection. Furthermore, the membrane was stable over 90 d of continuous operation. In a study by Grasso et al. [70], the modified functionalised graphene-based membrane, PVDF-f/G achieved close to 100% salt rejection while functionalised PVDF-f membrane obtained less salt rejection.

Table 2 summarises the recent studies on salt rejection performance and configuration used by graphene-based membranes. The average salt rejection of all graphene-based membranes was 99.6%, with he the lowest and the highest salt rejections were 98% and 100%, respectively. These results imply that regardless of MD configuration, the salt rejection performance by modified graphene-based membrane is outstanding due to its superior filtration ability, condensation rate of the permeate, porosity, and pore size compared to the bare membrane. The graphene also enhances the membrane's anti-fouling ability, which allows the delivery of stable permeate flux and a long lifespan for commercial application.

5.2. MD for others wastewater treatment

Besides desalination application, graphene-modified membrane in MD has been used for other applications such as treating coking wastewater [82], endotoxin removal [83], boron removal [56], and hydrogen isotopic water separation [84,85]. Ren et al. [82] investigated GO/PTFE composite membrane in treating biotreated coking wastewater (BCW) using direct contact membrane distillation (DCMD) configuration (Fig. 9a). It was discovered that the presence of a hydrophilic GO top layer repelled the hydrophobic organic compounds in BCW. Through the electrostatic interaction, the negatively charged GO layer increased the repulsive force toward the hydrophobic organics in BCW, reducing fouling and wetting tendencies. Besides that, GO nanochannels can block the large molecule in BCW and have a great affinity to liquid water (Fig. 9b). Thus, the GO hydrophilic top layer plays a big role as a protective barrier against the hydrophobic pollutants that can foul the membrane surface. The GO/PTFE hydrophilic (WCA of 77.5°)/hydrophobic

Table 2
Comparison of salt rejection performance with different graphene-based membranes and MD configurations

| MD configuration	Graphene-based formulation	NaCl feed concentration	Salt rejection (%)
DCMD	PVDF-PTFE + GO [66]	3.5–34.0 g L^{-1}	99.90
AGMD	(PVDF-*co*-HFP) (herein as PH) + GO [71]	3.5 wt.%	100.00
DCMD	PVDF-f + GO [70]	0.5 M	~100.00
VMD	PVDF + FTES-GO [68]	3.5 wt.%	99.90
AGMD	PVDF + GO [72]	35 g L^{-1}	>99.99
AGMD	PVDF + GQD3P (0.25 wt.%) [17]	3.5 wt.%	99.70
AGMD	PVDF + GO-APTS [73]	3.5 wt.%	99.90
AGMD	PVDF + GO-ODA (M2) [21]	3.5 wt.%	98.30
DCMD	PSF + GO (1.0 wt.%) [31]	2.5 wt.%	99.85
DCMD	PE + GNP [74]	RO brine solution	99.50
AGMD	PVDF + G [75]	RO brine solution	>99.90
SVGMD	PEDOT-PSS-G [76]	9.85 and 16.70 wt.%	> 99.60
DCMD	PVDF + MGNP [77]	0–30,000 ppm	>99.10
DCMD	PVDF-HFP + GO + ODS [78]	Seawater	>99.00
DCMD	PVDF + rGO-Bi$_2$WO$_6$ [79]	35 g L^{-1}	99.99
DCMD	PTFE + G [80]	70 g L^{-1}	>99.90
DCMD	PTFE + PVDF-G [81]	3,400–34,000 ppm	100.00
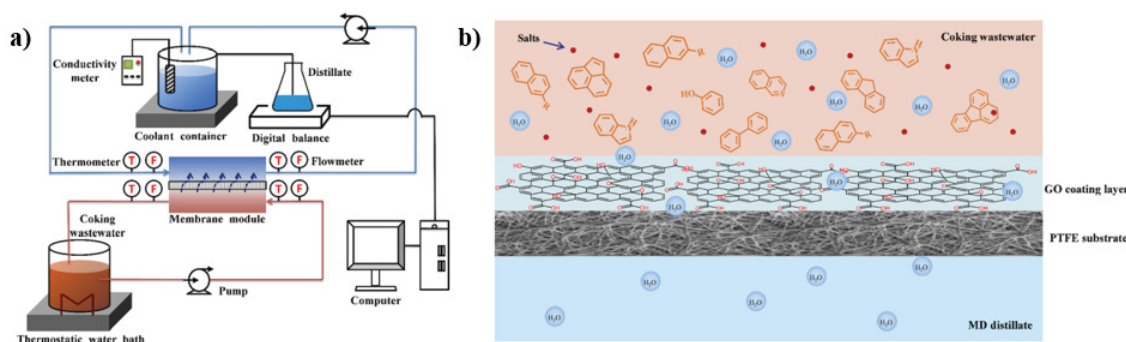
Fig. 9. Schematic diagram of (a) coking wastewater treatment using DCMD process and (b) mechanism of GO/PTFE composite membrane in treating BCW [82].

(WCA of 140.2°) composite membrane showed a high performance where 99% of salts and organics in BCW were removed, and the relative constant flux was 20 kg m^{-2} h^{-1}.

In the separation of hydrogen isotopes from water, Wen et al. [85] fabricated GO/rGO nanosheets grafted with perfluoroalkylsilanes (PFAS) using the air-gap membrane distillation configuration. The oxygen-containing group enhanced the membrane selectivity performance on the GO/rGO nanosheet with the mean separation factor of 1.067, WCA of 144°, and permeation flux of 0.47 kg m^{-2} h^{-1}. Besides that, Wen et al. [84] introduced layers of fluorinated silica nanoparticles on graphene oxide membrane (GOM) in production of a superhydrophobic membrane (WCA of 151°) to prevent water from passing through the membrane while permitting only pure vapour to pass through the membrane. Besides that, the GOM layer provided a nanochannel with high molecular sieving properties that enhanced the separation of molecules or ions. The membrane modification resulted in a high mean separation factor of 1.151 and permeation flux of 0.036 kg m^{-2} h^{-1}. Eryildiz et al. [56] synthesised PVDF nanofiber membrane with rGO using the electrospinning technique to remove boron from geothermal water. The membrane modification produced a high WCA of 124.5° that enhanced mass transfer (permeate water flux). The modified membranes also had better chemical and thermal stability than pure PVDF membrane. This rGO/PVDF membrane produced a high permeate flux of 29.9 L m^{-2} h^{-1}, 99.72% salt rejection, and 98.26% boron rejection.

In generating bacteria and endotoxin-free water, Gupta et al. [83] synthesised graphene oxide immobilised membrane (GOIM) on PTFE laminate supported on polypropylene composite membrane. It was the first research done in bacterial removal using a membrane distillation system. The GOIM had a WCA of 117°, lower than the bare PTFE membrane due to GO polar functional groups, but this reduction was insignificant. The higher water vapour flux for GOIM performance was because the nanocarbon on the membrane surface acted as sorbent sites, thus enhancing water vapour diffusion and preventing the liquid from passing through the membrane pore. In the antibacterial activity, GO nanosheet trapped the bacteria, and this contact altered the bacteria dramatically due to the oxidative stress shown in Fig. 10. The performance of the GOIM membrane was 27.6 kg m^{-2} h^{-1} for flux and 99.9% for boron removal efficiency.

From the studies, the graphene in the membrane distillation for wastewater treatment application can repel the hydrophobic organic compounds with its hydroxyl group, reducing fouling and wetting tendencies. It also has high filtration ability and high molecular sieving properties that enhance the separation of molecules or ions, with the addition of bacterial removal properties.

6. Surface properties and performances of graphene-modified membranes for MD

Based on a study by Woo et al. [71], to obtain a robust, superhydrophobic membrane for membrane distillation, 1–10 wt.% of GO which was synthesised via electrospinning and 18 wt.% of polyvinylidene fluoride-*co*-hexafluoropropylene (PVDF-*co*-HFP, herein as PH) were chosen.
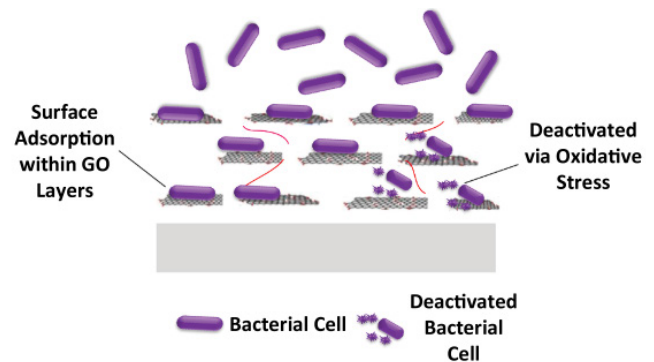

Fig. 10. Mechanism of bacterial deactivation by GOIM during membrane distillation process [83].

The contact angle of both membranes was measured using a sessile drop method, and five measurements were taken for each membrane. The average contact angle for the best GO sample and PH were 162.7° and 142.3°, respectively. Fig. 11a shows that the contact angle values for all the GO samples were higher than that of PH membrane. The poor contact angle on PH membrane caused it to have a wetting problem in less than 3 h while GO, having a hydrophobicity property, resulted in good stability for 20 h. Zahirifar et al. [21] obtained 146° for modified graphene-membrane and 77° for unmodified PVDF membrane. Woo et al. [75] tested graphene/PVDF flat-sheet membrane for treating brine using AGMD. The result shows that neat PVDF membrane had lower water flux than GO, recording 11.6 and 20.5 L m^{-2} h^{-1}, respectively. The same results were obtained by Seo et al. [80], where permeate flux by PTFE-GO and pristine PTFE were 50 and 14.2 LMH, respectively.

In hydrophobic modification of graphene oxide membrane, Mao et al. [86] first prepared a pure graphene membrane with a WCA of 48.9° as the pure GO NP is hydrophilic. Then, the second modification was done by immersing the membrane in hexadecyltrimethoxysilane (HDTMS) solution. This step was able to increase the WCA to 73.2°, but it was still a hydrophilic membrane. Thus, the third modification was by intercalating the GO NPs with SiO$_2$ NPs, filtered on PAN substrate, followed by treatment with HDTMS solution. This procedure enhanced the membrane hydrophobicity up to 120.8° as shown in Fig. 11b. The optimised graphene oxide membrane exhibited a water flux of 13.59 kg m^{-2} h^{-1} and salt rejection of 99.99% in VMD process.

Wen et al. [84] first sprayed GO-membranes with fluorinated silica NPs to produce a modified membrane with 164° WCA. Then, the fluoro-containing resin was sprayed on the membrane to enhance the adhesion between graphene oxide membrane and fluorinated silica NPs, even though the resulting WCA slightly dropped to 150°. The membrane surface modification was shown in Fig. 11c.

Table 3 summarises the recent studies on contact angle and permeate flux using graphene-based membranes. The average contact angle obtained was 118° while the average permeates flux was 38.65 LMH. It can be concluded that in MD, a hydrophobic modifier such as octadecyltrichlorosilane (ODS) and octadecylamine (ODA) might be needed to increase the membrane's water contact angle.
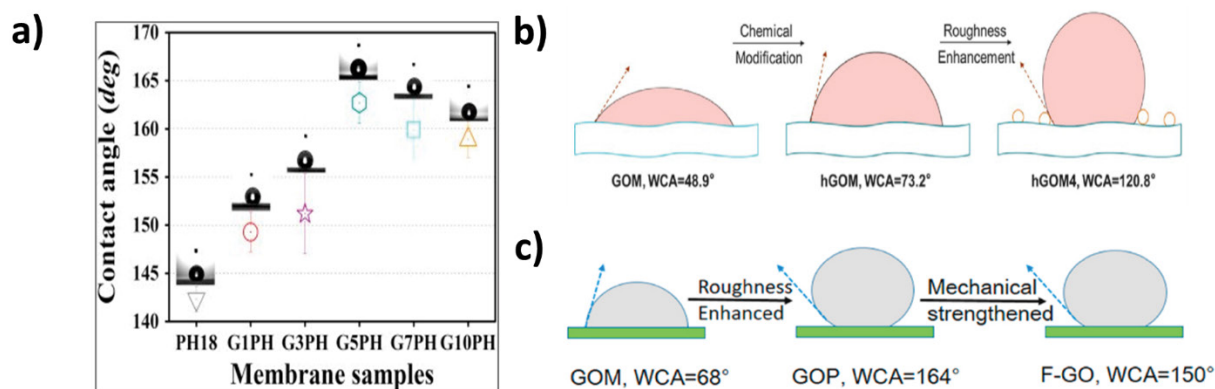
Fig. 11. (a) Contact angles with different types of membrane samples [71], (b) graphene oxide membrane hydrophobic modification [86] and (c) graphene oxide membrane superhydrophobic modification [84].

Table 3
Comparison of contact angle and permeate flux of various graphene-based membranes

Membrane	Contact angle (°)	Permeate flux (kg m^{-2} h^{-1})	Finding
PVDF-PTFE + GO [66]	90.6 ± 2.1	97.0	Hydrophobic GO nanopore structure created an almost frictionless surface for water flow, contributed to high permeate flux.
(PVDF-co-HFP (PH) + GO [71]	162.0	22.9 L m^{-2} h^{-1}	Modified membrane increased permeate flux compared to bare membrane.
PVDF + GO [87]	129.3 ± 1	~24.5	Modification on membrane show that GO NPs attached on the internal surface of the membrane pores rather than on membrane external surface.
PVDF + FTES-GO [68]	132.5	36.4	Grafted GO nanosheets created rougher surface and increased contact angle.
PVDF + GO-ODA (M2) [21]	146.0 ± 1.1	16.7	GO-ODA formed interconnected nanochannels and enhanced permeate flux.
PSF + GO (2 wt.%) [31]	83.0 ± 0.94	22.8 L m^{-2} h^{-1}	Addition of GO provided good porosity, pore size and hydrophobic for separation process.
PE + GNP (0.16 wt.%) [74]	122.6	16.7 L m^{-2} h^{-1}	Contact angle of the modified membrane increased with additional GNP, but it can't be high as it will result in a slight agglomeration that can turn the membrane hydrophilic.
PVDF + G (0.5%) [75]	87.2 ± 2.5	20.5 L m^{-2} h^{-1}	Contact angle of the modified membrane increased but increasing the graphene NPs concentration caused the membrane to have smaller pore size, lower porosity and thicker thickness due to the aggregation of the graphene NPs.
PVDF + GO-PVP [88]	145.2	0.65	GO-PVP/PVDF membrane resulted in higher permeate flux and fouling-resistant compared to the pristine PVDF membrane.
PVDF + MGNP [77]	141.3 ± 1.2	19.8	graphene nanoplatelet filler increased the membrane LEP value and also the WCA by over 10°.
PTFE + PVDF-G [81]	75.0 ± 2	64.5	Hydrophilicity on the permeate side resulting in rapid condensation and removal of the permeate and thus, increase the permeate flux.
PVDF-HFP + GO + ODS [78]	162.0 ± 1.7	34.1 ± 0.96 L m^{-2} h^{-1}	GO provided hierarchical roughness while OH functional groups ensured the uniform functionalisation by ODS for superhydrophobic membrane surface modification.

7. Graphene-based photothermal membrane for MD

Despite MD having low operating temperature, conventional MD has several drawbacks. According to Martínez-Díez and Vázquez-González [89], the mechanism behind conventional MD requires heating bulk water at the same temperature. This will result in interfacial temperature polarisation since the water evaporated at the membrane of MD removes the latent heat. Subsequently, it will cause a low net driving force for MD membrane to transport the water since the interfacial temperature polarisation decreases the membrane temperature [9]. A concept design of solar thermal interfacial heating and MD has been proposed to alleviate these drawbacks. Based on Fig. 12a, only interfacial source water on the photothermal layer will be heated and gains thermal energy from the sunlight. The vapour of the source water then will flow through the photothermal layer and membrane, while the condensate will become the distillate water [90]. Photothermal membrane for solar-driven interfacial heating consists of two main components: (i) microporous hydrophobic membrane and (ii) photothermal nanomaterial layer used to utilise solar energy. Photothermal materials can soak up light and transform it into thermal energy [91]. The solar irradiation on Earth has its solar spectrum range, encompassing the ultraviolet, visible, and near-infrared regions at 3%, 45%, and 52%, respectively [82] (Fig. 12b) [92].

Many studies have shown graphene as a remarkable photothermal nanomaterial that can be used for solar-driven membrane distillation. This is because graphene has excellent light-absorbing properties and a low-cost, scalable fabrication process. The graphene-based membrane provided ultrafast water-permeable channels and a high salt resistance network [93,94]. Huang et al. [94] proposed a photothermal MD evaporation system shown in Fig. 13. It was observed that the absorption efficiency of rGO/rGO-PTFE membrane was more than 80% which was considered high under normal solar illumination, and achieved as much as 78.6% water transmembrane flux enhancement compared to bare PTFE membrane.

Hou et al. [95] demonstrated the application of GO incorporated with mixed cellulose ester (MCE) films for solar desalination using vacuum filtration. After being exposed to a light density of one sun, the seawater weight loss recorded was 0.68 kg m⁻². Besides having an excellent thermal efficiency, the membrane also exhibited good stability as the weight loss values of seawater after eight cycles were linearly fitted to a straight line. The GO/MCE also had good recyclability, and the purified water fully met the drinking water standard by the World Health Organisation (WHO).

Table 4 compares the evaporation rate and solar conversion by various graphene photothermal membranes. The average solar conversion efficiency was 85.28%, with the lowest and the highest solar conversions were at 48.20% and 94.20%, respectively. Graphene-based material has a high solar absorption ability where it can absorb more than 99% of the whole sunlight. As the graphene-based membrane has high porosity, it enables fast water transport while lowering heat loss to bulk water. These properties make graphene as an excellent material for photothermal membrane distillation application.
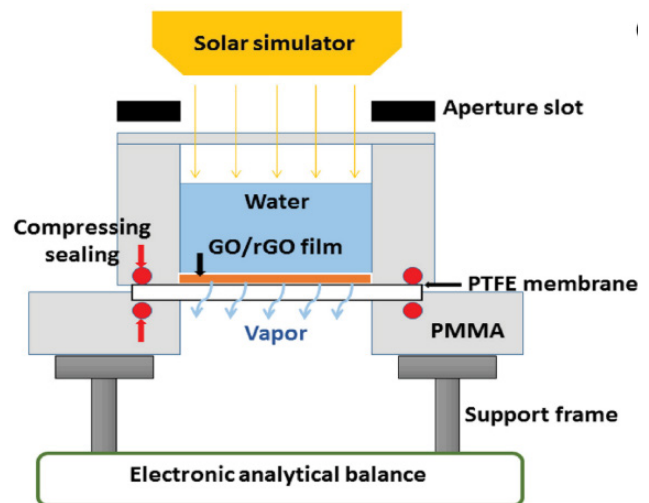

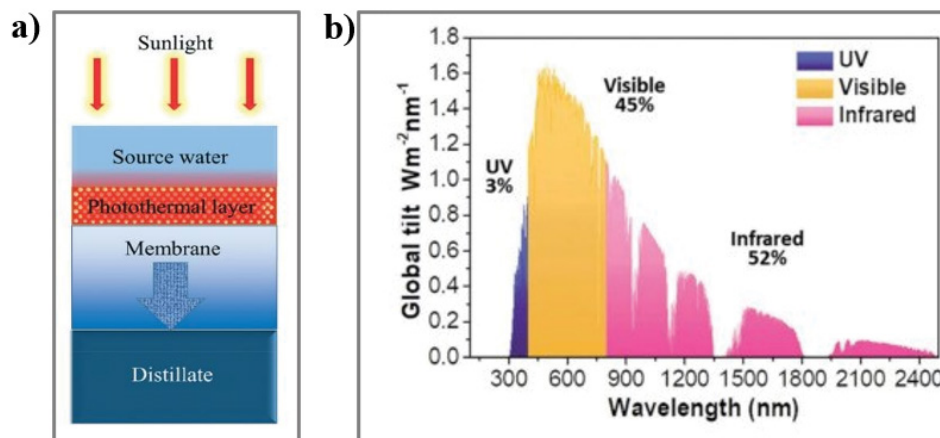Fig. 13. Photothermal membrane distillation setup [94].

Fig. 12. Schematic diagram of (a) solar interfacial membrane distillation [71] and (b) solar spectral irradiance [92].

Table 4
Comparison of evaporation rate and solar conversion efficiency of various graphene-based membranes

Membrane	Graphene content (wt.%)	Evaporation rate (kg m^{-2} h^{-1})	Solar irradiance (W m^{-2})	Solar conversion efficiency (%)	Finding
GO/CNT-silica Janus [96]	–	1.30	1.0	74.00	GO/CNTs layer enhanced light absorption while the electrospun silica membrane provided thermal insulation and water channel.
rGO-agarose/cotton aerogel shell [97]	0.4 g	4.00	1.0	>97% light absorption	Cotton cores absorbed and stored a large amount of water, while photothermal rGO-agarose-cotton aerogel sheet served as water retainer and light absorber.
GO/SA PAM-PVA hydrogel [98]	–	1,274.2 g m^{-2}	1.0	–	Hydrogel showed excellent solar evaporation properties due to GO NPs solar absorber.
Graphite powder (GP) and a semiper-meable collodion membrane (SCM) [99]	8 mg	1.36	1.5	56.80	GP/SCM showed good light absorber properties. Can be reused over 20 cycles, showing its long-term application.
Al foil/rGO/Mn$_3$O$_4$ film [100]	0.18 g	1.65	1.0	90.00	Successful combination of rGO/Mn$_3$O$_4$ resulted in an excellent solar absorption of more than 99% of the whole sunlight.
Monolithic bilayer sheets (MBS) of hierarchically porous graphitic carbon (HPGC) [101]	–	1.34	1.0	83.20	HPGC showed excellent solar absorption where it absorbed ~97% broadband of solar illumination.
GO/PVA EFMs [102]	1–6 wt.% PVA	1.42	1.0	94.20	Besides photothermal properties, the membrane displayed excellent stability suitable for long-term photothermal evaporation.
rGO on top of polystyrene (PS) [103]	–	1.31	1.0	83.00	rGO provided a porous structure on the top layer with strong light absorption ability to enhance the permeate flux.
CB/GO (body), GO pillars (tentacles), expanded polystyrene (EPS) matrix [104]	500 mg	1.27	1.0	87.50	CB/GO layer with porous structures showed high light absorption and vertically printed porous GO pillars enabled fast water transport and lowering heat loss to bulk water.
rGO [105]	400 mg	1.14	1.0	90.20	Increase of reduction degree of rGO resulted in higher evaporation efficiency.
CG/GN [106]	320 mg	1.25	1.0	85.60	CNT/GO showed high solar absorption (>97%) and open porous structure for vapour escape to enhance the evaporation flux.

8. Conclusion

Permeate flux decline, membrane fouling, and wetting are severe challenges faced in MD operations. Thus, various studies have been carried out in recent years to modify the MD membranes by incorporating nanomaterials, particularly graphene, to overcome these challenges and enhance the performances of MD. This review provides a comprehensive evaluation of the incorporation of graphene in the MD. The desired characteristics of the membrane for MD operations, such as a higher LEP, permeability, porosity, hydrophobicity, chemical stability, thermal conductivity, and mechanical strength have been thoroughly discussed. This review also summarises different aspects of graphene-based membranes for MD and how it affects the performance of MD. Generally, the graphene-modified membranes are more hydrophobic with a higher contact angle. In addition, due to the nanostructure of graphene pores, the salt rejection is typically higher while maintaining the flux. Graphene-based membranes also have high solar absorbance properties where they can substantially improve the photothermal MD application.

Despite the tremendous progress observed for graphene-based MD, several challenges still need to be resolved, particularly on the development of membrane with finely tuned microstructures and controlled pore size or inter-layer spacing. In addition to that, the graphene-based membrane for MD is only developed at a lab scale. Thus, the graphene-based membrane must be fabricated in balance with efficiency, cost, scalability, stability, and adaptability to make it commercially viable. Most of the work conducted on graphene-based MD is mainly for salt rejection. As such, there is still minimal information on the graphene-based MD for other applications such as oil rejection and wastewater treatment. Monitoring the long-term stability of graphene-based membranes under practical applications is also essential for future adaptation.

Acknowledgement

References

[1] M. Kummu, J.H.A. Guillaume, H. de Moel, S. Eisner, M. Flörke, M. Porkka, S. Siebert, T.I.E. Veldkamp, P.J. Ward, The world's road to water scarcity: shortage and stress in the 20th century and pathways towards sustainability, Sci. Rep., 6 (2016) 1–16, doi: 10.1038/srep38495.

[2] N.H. Othman, N.H. Alias, N.S. Fuzil, F. Marpani, M.Z. Shahruddin, C.M. Chew, K.M.D. Ng, W.J. Lau, A.F. Ismail, A review on the use of membrane technology systems in developing countries, Membranes (Basel), 12 (2022), doi: 10.3390/membranes12010030.

[3] B.L. Pangarkar, M.G. Sane, M. Guddad, Reverse osmosis and membrane distillation for desalination of groundwater: a review, ISRN Mater. Sci., 2011 (2011) 1–9.

[4] H. Al Maawali, D.J. Kayode Adewole, A. Al Kharusi, J. Al-Qartoubi, M. Al Maamari, R. Al Balushi, R. Al Mazrui, Comparative studies of membrane distillation and reverse osmosis for seawater desalination, J. Stud. Res., 10 (2021), doi: 10.47611/jsr.v10i2.1208.

[5] H.S. Son, S. Soukane, J. Lee, Y. Kim, Y.D. Kim, N. Ghaffour, Towards sustainable circular brine reclamation using seawater reverse osmosis, membrane distillation and forward osmosis hybrids: an experimental investigation, J. Environ. Manage., 293 (2021), doi: 10.1016/j.jenvman.2021.112836.

[6] A. Ali, R.A. Tufa, F. Macedonio, E. Curcio, E. Drioli, Membrane technology in renewable-energy-driven desalination, Renewable Sustainable Energy Rev., 81 (2018) 1–21.

[7] E. Mendez, Sustainable desalination: membrane distillation delivers greener clean water, Filtr. Sep., 49 (2012) 26–28.

[8] I.A. Said, N. Fuentes, Z. He, R. Xin, K. Zuo, Q. Li, Low-cost desalination of seawater and hypersaline brine using nanophotonics enhanced solar energy membrane distillation, Environ. Sci. Water Res. Technol., 6 (2020) 2180–2196.

[9] A. Alkhudhiri, N. Darwish, N. Hilal, Membrane distillation: a comprehensive review, Desalination, 287 (2012) 2–18.

[10] N.S. Fuzil, N.H. Othman, N.H. Alias, F. Marpani, M.H.D. Othman, A.F. Ismail, W.J. Lau, K. Li, T.D. Kusworo, I. Ichinose, M.M.A. Shirazi, A review on photothermal material and its usage in the development of photothermal membrane for sustainable clean water production, Desalination, 517 (2021) 115259, doi: 10.1016/j.desal.2021.115259.

[11] M.I. Siyal, C.K. Lee, C. Park, A.A. Khan, J.O. Kim, A review of membrane development in membrane distillation for emulsified industrial or shale gas wastewater treatments with feed containing hybrid impurities, J. Environ. Manage., 243 (2019) 45–66.

[12] R. Schwantes, J. Seger, L. Bauer, D. Winter, T. Hogen, J. Koschikowski, S.U. Geißen, Characterization and assessment of a novel plate and frame md module for single pass wastewater concentration–feed gap air-gap membrane distillation, Membranes (Basel), 9 (2019), doi: 10.3390/membranes9090118.

[13] L.N. Nthunya, L. Gutierrez, S. Derese, E.N. Nxumalo, A.R. Verliefde, B.B. Mamba, S.D. Mhlanga, A review of nanoparticle-enhanced membrane distillation membranes: membrane synthesis and applications in water treatment, J. Chem. Technol. Biotechnol., 94 (2019) 2757–2771.

[14] S.O. Olatunji, L.M. Camacho, Heat and mass transport in modeling membrane distillation configurations: a review, Front. Energy Res., 6 (2018) 1–18.

[15] G. Li, L. Lu, Modeling and performance analysis of a fully solar-powered stand-alone sweeping gas membrane distillation desalination system for island and coastal households, Energy Convers. Manage., 205 (2020) 112375, doi: 10.1016/j.enconman.2019.112375.

[16] H. Du, S. Bandara, L.E. Carson, R.R. Kommalapati, Association of Polyethylene Glycol Solubility with Emerging Membrane Technologies, Wastewater Treatment, and Desalination, K. Summers, Ed., Water Quality, 2020, doi: 10.5772/intechopen.89060.

[17] A. Jafari, M.R.S. Kebria, A. Rahimpour, G. Bakeri, Graphene quantum dots modified polyvinylidenefluride (PVDF) nanofibrous membranes with enhanced performance for air-gap membrane distillation, Chem. Eng. Process. Process Intensif., 126 (2018) 222–231.

[18] M.R.S. Kebria, A. Rahimpour, G. Bakeri, R. Abedini, Experimental and theoretical investigation of thin ZIF-8/chitosan coated layer on air-gap membrane distillation performance of PVDF membrane, Desalination, 450 (2019) 21–32.

[19] D. Ghim, X. Wu, M. Suazo, Y.S. Jun, Achieving maximum recovery of latent heat in photothermally driven multi-layer stacked membrane distillation, Nano Energy, 80 (2021) 105444, doi: 10.1016/j.nanoen.2020.105444.

[20] I.A. Said, T.R. Chomiak, Z. He, Q. Li, Low-cost high-efficiency solar membrane distillation for treatment of oil produced waters, Sep. Purif. Technol., 250 (2020), doi: 10.1016/j.seppur.2020.117170.

[21] J. Zahirifar, S.M.A. Moosavian, A. Hadi, P. Khadiv-Parsi, J. Karimi-Sabet, Fabrication of a novel octadecylamine functionalized graphene oxide/PVDF dual-layer flat sheet membrane for desalination via air-gap membrane distillation, Desalination, 428 (2018) 227–239.

[22] V. Murugesan, D. Rana, T. Matsuura, C.Q. Lan, Optimization of nanocomposite membrane for vacuum membrane distillation (VMD) using static and continuous flow cells: effect of nanoparticles and film thickness, Sep. Purif. Technol., 241 (2020), doi: 10.1016/j.seppur.2020.116685.

[23] J. Swaminathan, H.W. Chung, D.M. Warsinger, J.H. Lienhard V, Energy efficiency of membrane distillation up to high salinity: evaluating critical system size and optimal membrane thickness, Appl. Energy, 211 (2018) 715–734.

[24] Z.S. Tai, M.H.A. Aziz, M.H.D. Othman, A.F. Ismail, M.A. Rahman, J. Jaafar, Chapter 8 – An Overview of Membrane Distillation, A.F. Ismail, M.A. Rahman, M.H.D. Othman, T. Matsuura, Eds., Membrane Separation Principles and Applications: From Material Selection to Mechanisms and Industrial Uses, Handbooks in Separation Science, Elsevier, Netherlands, 2019, pp. 251–281.

[25] X. Li, L. Deng, X. Yu, M. Wang, X. Wang, C. García-Payo, M. Khayet, A novel profiled core-shell nanofibrous membrane for wastewater treatment by direct contact membrane distillation, J. Mater. Chem. A, 4 (2016) 14453–14463.

[26] H.R. Mortaheb, M. Baghban Salehi, M. Rajabzadeh, Optimized hybrid PVDF/graphene membranes for enhancing performance of AGMD process in water desalination, J. Ind. Eng. Chem., 99 (2021) 407–421.

[27] S. Sifat, M. Membran, K. Rata, P. Vinilidena, T. Kesan, K. Polimer, A.M. Nasib, I. Hatim, N. Jullok, H.R. Alamery, Morphological properties of poly(vinylidene fluoride-*co*-tetrafluoroethylene) membrane: effect of solvents and polymer concentrations, Malaysian J. Anal. Sci., 21 (2017) 356–364.

[28] T. Pan, J. Liu, N. Deng, Z. Li, L. Wang, Z. Xia, J. Fan, Y. Liu, ZnO Nanowires@PVDF nanofiber membrane with superhydrophobicity for enhanced anti-wetting and anti-scaling properties in membrane distillation, J. Membr. Sci., 621 (2021) 118877, doi: 10.1016/j.memsci.2020.118877.

[29] A. Kullab, Desalination using Membrane Distillation: Experimental and Numerical Study, Doctoral Thesis, Comprehensive Summary (Other Academic), KTH Royal Institute of Technology, Stockholm, 2011. Avaialble at: http://kth.diva-portal.org/smash/get/diva2:450562/FULLTEXT01.pdf%0Ahttp://urn.kb.se/resolve?urn=urn:nbn:se:kth:diva-44405

[30] M.M.A. Shirazi, S. Bazgir, F. Meshkani, A dual-layer, nanofibrous styrene-acrylonitrile membrane with hydrophobic/hydrophilic composite structure for treating the hot dyeing effluent by direct contact membrane distillation, Chem. Eng. Res. Des., 164 (2020) 125–146.

[31] L.M. Camacho, T.A. Pinion, S.O. Olatunji, Behavior of mixed-matrix graphene oxide – polysulfone membranes in the process of direct contact membrane distillation, Sep. Purif. Technol., 240 (2020) 116645, doi: 10.1016/j.seppur.2020.116645.

[32] Z. Li, Z.L. Xu, B.Q. Huang, Y.X. Li, M. Wang, Three-channel stainless steel hollow fiber membrane with inner layer modified by nano-TiO$_2$ coating method for the separation of oil-in-water emulsions, Sep. Purif. Technol., 222 (2019) 75–84.

[33] X.M. Tan, D. Rodrigue, A review on porous polymeric membrane preparation. Part II: Production techniques with polyethylene, polydimethylsiloxane, polypropylene, polyimide, and polytetrafluoroethylene, Polymers (Basel), 11 (2019), doi: 10.3390/polym11081310.

[34] L. Eykens, K. De Sitter, C. Dotremont, L. Pinoy, B. Van der Bruggen, Membrane synthesis for membrane distillation: a review, Sep. Purif. Technol., 182 (2017) 36–51.

[35] C. Fang, W. Liu, P. Zhang, M. Yao, S. Rajabzadeh, N. Kato, H. Kyong Shon, H. Matsuyama, Controlling the inner surface pore and spherulite structures of PVDF hollow fiber membranes in thermally induced phase separation using triple-orifice spinneret for membrane distillation, Sep. Purif. Technol., 258 (2021) 117988, doi: 10.1016/j.seppur.2020.117988.

[36] M. Reza Shirzad Kebria, A. Rahimpour, Membrane Distillation: Basics, Advances, and Applications, A. Abdelrasoul, Ed., Advances in Membrane Technologies, IntechOpen, 2020, pp. 1–21. Available at: https://doi.org/10.5772/intechopen.86952

[37] W. Qing, J. Wang, X. Ma, Z. Yao, Y. Feng, X. Shi, F. Liu, P. Wang, C.Y. Tang, One-step tailoring surface roughness and surface chemistry to prepare superhydrophobic polyvinylidene fluoride (PVDF) membranes for enhanced membrane distillation performances, J. Colloid Interface Sci., 553 (2019) 99–107.

[38] X. Gong, Y. Meng, J. Zhu, X. Wang, J. Lu, Y. Cheng, Y. Tao, H. Wang, Construct a stable super-hydrophobic surface through acetonitrile extracted lignin and nano-silica and its application in oil-water separation, Ind. Crops Prod., 166 (2021) 113471, doi: 10.1016/j.indcrop.2021.113471.

[39] H. Li, H. Liu, W. Shi, H. Zhang, R. Zhou, X. Qin, Preparation of hydrophobic zeolitic imidazolate framework-71 (ZIF-71)/PVDF hollow fiber composite membrane for membrane distillation through dilute solution coating, Sep. Purif. Technol., 251 (2020) 117348, doi: 10.1016/j.seppur.2020.117348.

[40] K. Li, K. Wang, Y. Zhang, H. Liu, J. Wang, A polyvinylidene fluoride (PVDF)–silica aerogel (SiAG) insulating membrane for improvement of thermal efficiency during membrane distillation, J. Membr. Sci., 597 (2020) 117632, doi: 10.1016/j.memsci.2019.117632.

[41] J. Li, L.F. Ren, H.S. Zhou, J. Yang, J. Shao, Y. He, Fabrication of superhydrophobic PDTS-ZnO-PVDF membrane and its anti-wetting analysis in direct contact membrane distillation (DCMD) applications, J. Membr. Sci., 620 (2020) 118924, doi: 10.1016/j.memsci.2020.118924.

[42] Y.Z. Tan, H. Wang, L. Han, M.B. Tanis-Kanbur, M.V. Pranav, J.W. Chew, Photothermal-enhanced and fouling-resistant membrane for solar-assisted membrane distillation, J. Membr. Sci., 565 (2018) 254–265.

[43] A.A. Khan, M.I. Siyal, J.O. Kim, Fluorinated silica–modified anti–oil-fouling omniphobic F–SiO$_2$@PES robust membrane for multiple foulants feed in membrane distillation, Chemosphere, 263 (2021) 128140, doi: 10.1016/j.chemosphere.2020.128140.

[44] S. Gupta, B. Evans, Interplay of graphene oxide and interfacial polymerized polyamide-crosslinked thin-film composite membranes for enhanced performance during reverse osmosis, Desal. Water Treat., 218 (2021) 177–192.

[45] J.C. Slonczewski, P.R. Weiss, Band structure of graphite, Phys. Rev., 109 (1958) 272–279.

[46] P.S. Goh, A.F. Ismail, Graphene-based nanomaterial: the state-of-the-art material for cutting edge desalination technology, Desalination, 356 (2015) 115–128.

[47] A. Aghigh, V. Alizadeh, H.Y. Wong, M.S. Islam, N. Amin, M. Zaman, Recent advances in utilization of graphene for filtration and desalination of water: a review, Desalination, 365 (2015) 389–397.

[48] V.-D. Dao, H.-S. Choi, Carbon-based sunlight absorbers in solar-driven steam generation devices, Global Challenges, 2 (2018) 1700094, doi: 10.1002/gch2.201700094.

[49] H. Ren, M. Tang, B. Guan, K. Wang, J. Yang, F. Wang, M. Wang, J. Shan, Z. Chen, D. Wei, H. Peng, Z. Liu, Hierarchical graphene foam for efficient omnidirectional solar–thermal energy conversion, Adv. Mater., 29 (2017) 1–7.

[50] M.F. Zainuddin, N.H. Nik Raikhan, N.H. Othman, W.F.H. Abdullah, Synthesis of reduced graphene oxide (rGO) using different treatments of graphene oxide (GO), IOP Conf. Ser.: Mater. Sci. Eng., 358 (2018) 012046, doi: 10.1088/1757-899X/358/1/012046.

[51] A. Tuantranont, Nanomaterials for Sensing Applications: Introduction and Perspective, A. Tuantranont, Ed., Applications of Nanomaterials in Sensors and Diagnostics. Springer Series on Chemical Sensors and Biosensors, Springer, Berlin, Heidelberg, 2012, pp. 1–16. Available at: https://doi.org/10.1007/5346_2012_41

[52] A.M. Nasir, P.S. Goh, A.F. Ismail, Chapter 3 – Synthesis Route for the Fabrication of Nanocomposite Membranes, M. Sadrzadeh, T. Mohammadi, Eds., Nanocomposite Membranes for Water and Gas Separation: Micro and Nano Technologies, Elsevier Inc., Netherlands, 2019. Available at: https://doi.org/10.1016/B978-0-12-816710-6.00003-1

[53] N.F.D. Junaidi, N.H. Othman, N.S. Fuzil, M.S. Mat Shayuti, N.H. Alias, M.Z. Shahruddin, F. Marpani, W.J. Lau, A.F. Ismail, N.F.D. Aba, Recent development of graphene oxide-based

membranes for oil–water separation: a review, Sep. Purif. Technol., 258 (2021) 118000, doi: 10.1016/j.seppur.2020.118000.

[54] N.F D. Junaidi, N.A. Khalil, A.F. Jahari, N. Kassim Shaari, M. Shahruddin, N.H. Alias, N. Othman, Effect of graphene oxide (GO) on the surface morphology & hydrophilicity of polyethersulfone (PES), IOP Conf. Ser.: Mater. Sci. Eng., 358 (2018) 012047, doi: 10.1088/1757-899X/358/1/012047.

[55] A. Alammar, S.H. Park, C.J. Williams, B. Derby, G. Szekely, Oil-in-water separation with graphene-based nanocomposite membranes for produced water treatment, J. Membr. Sci., 603 (2020) 118007, doi: 10.1016/j.memsci.2020.118007.

[56] B. Eryildiz, B. Ozbey-Unal, E. Gezmis-Yavuz, D.Y. Koseoglu-Imer, B. Keskinler, I. Koyuncu, Flux-enhanced reduced graphene oxide (rGO)/PVDF nanofibrous membrane distillation membranes for the removal of boron from geothermal water, Sep. Purif. Technol., 274 (2021) 119058, doi: 10.1016/j.seppur.2021.119058.

[57] M.S. Salem, A.H. El-Shazly, N. Nady, M.R. Elmarghany, M.N. Sabry, PES/PVDF blend membrane and its composite with graphene nanoplates: preparation, characterization, and water desalination via membrane distillation, Desal. Water Treat., 166 (2019) 9–23.

[58] R.J. Kadhim, F.H. Al-Ani, M. Al-Shaeli, Q.F. Alsalhy, A. Figoli, Removal of dyes using graphene oxide (GO) mixed matrix membranes, Membranes (Basel), 10 (2020) 1–24.

[59] N.G.P. Chew, S. Zhao, C. Malde, R. Wang, Superoleophobic surface modification for robust membrane distillation performance, J. Membr. Sci., 541 (2017) 162–173.

[60] A.F.M. Ibrahim, Y.S. Lin, Synthesis of graphene oxide membranes on polyester substrate by spray coating for gas separation, Chem. Eng. Sci., 190 (2018) 312–319.

[61] M.I. Baig, P.G. Ingole, J. Deok Jeon, S.U. Hong, W.K. Choi, H.K. Lee, Water vapor transport properties of interfacially polymerized thin film nanocomposite membranes modified with graphene oxide and GO-TiO$_2$ nanofillers, Chem. Eng. J., 373 (2019) 1190–1202.

[62] F. Li, Z. Yu, H. Shi, Q. Yang, Q. Chen, Y. Pan, G. Zeng, L. Yan, A Mussel-inspired method to fabricate reduced graphene oxide/g-C$_3$N$_4$ composites membranes for catalytic decomposition and oil-in-water emulsion separation, Chem. Eng. J., 322 (2017) 33–45.

[63] A. Hassanpour, S. Nahar, X. Tong, G. Zhang, M.A. Gauthier, S. Sun, Photocatalytic interlayer spacing adjustment of a graphene oxide/zinc oxide hybrid membrane for efficient water filtration, Desalination, 475 (2020) 114174, doi: 10.1016/j.desal.2019.114174.

[64] X. Zhang, Z. Zhang, Z. Zeng, S. Du, E. Liu, Superoleophobic graphene oxide/halloysite nanotube composite membranes for oil-water separation, Mater. Chem. Phys., 263 (2021) 124347, doi: 10.1016/j.matchemphys.2021.124347.

[65] K. Guan, J. Shen, G. Liu, J. Zhao, H. Zhou, W. Jin, Spray-evaporation assembled graphene oxide membranes for selective hydrogen transport, Sep. Purif. Technol., 174 (2017) 126–135.

[66] M. Bhadra, S. Roy, S. Mitra, Desalination across a graphene oxide membrane via direct contact membrane distillation, Desalination, 378 (2016) 37–43.

[67] M. Fouladivanda, J. Karimi-Sabet, F. Abbasi, M.A. Moosavian, Step-by-step improvement of mixed-matrix nanofiber membrane with functionalized graphene oxide for desalination via air-gap membrane distillation, Sep. Purif. Technol., 256 (2021) 117809, doi: 10.1016/j.seppur.2020.117809.

[68] H. Li, W. Shi, X. Zeng, S. Huang, H. Zhang, X. Qin, Improved desalination properties of hydrophobic GO-incorporated PVDF electrospun nanofibrous composites for vacuum membrane distillation, Sep. Purif. Technol., 230 (2020) 115889, doi: 10.1016/j.seppur.2019.115889.

[69] Z. Xu, X. Yan, Z. Du, J. Li, F. Cheng, Effect of oxygenic groups on desalination performance improvement of graphene oxide-based membrane in membrane distillation, Sep. Purif. Technol., 251 (2020) 117304, doi: 10.1016/j.seppur.2020.117304.

[70] G. Grasso, F. Galiano, M.J. Yoo, R. Mancuso, H.B. Park, B. Gabriele, A. Figoli, E. Drioli, Development of graphene-PVDF composite membranes for membrane distillation, J. Membr. Sci., 604 (2020) 118017, doi: 10.1016/j.memsci.2020.118017.

[71] Y.C. Woo, L.D. Tijing, W.G. Shim, J.S. Choi, S.H. Kim, T. He, E. Drioli, H.K. Shon, Water desalination using graphene-enhanced electrospun nanofiber membrane via air-gap membrane distillation, J. Membr. Sci., 520 (2016) 99–110.

[72] A. Abdel-Karim, J.M. Luque-Alled, S. Leaper, M. Alberto, X. Fan, A. Vijayaraghavan, T.A. Gad-Allah, A.S. El-Kalliny, G. Szekely, S.I.A. Ahmed, S.M. Holmes, P. Gorgojo, PVDF membranes containing reduced graphene oxide: effect of degree of reduction on membrane distillation performance, Desalination, 452 (2019) 196–207.

[73] S. Leaper, A. Abdel-Karim, B. Faki, J.M. Luque-Alled, M. Alberto, A. Vijayaraghavan, S.M. Holmes, G. Szekely, M.I. Badawy, N. Shokri, P. Gorgojo, Flux-enhanced PVDF mixed matrix membranes incorporating APTS-functionalized graphene oxide for membrane distillation, J. Membr. Sci., 554 (2018) 309–323.

[74] S. Mansour, A. Giwa, S.W. Hasan, Novel graphene nanoplatelets-coated polyethylene membrane for the treatment of reject brine by pilot-scale direct contact membrane distillation: an optimization study, Desalination, 441 (2018) 9–20.

[75] Y.C. Woo, Y. Kim, W.G. Shim, L.D. Tijing, M. Yao, L.D Nghiem, J.S. Choi, S.H. Kim, H.K. Shon, Graphene/PVDF flat-sheet membrane for the treatment of RO brine from coal seam gas produced water by air-gap membrane distillation, J. Membr. Sci., 513 (2016) 74–84.

[76] B. Gong, H. Yang, S. Wu, G. Xiong, J. Yan, K. Cen, Z. Bo, K. Ostrikov, Graphene array-based anti-fouling solar vapour gap membrane distillation with high energy efficiency, Nano-Micro Lett., 11 (2019) 1–14.

[77] M.S. Salem, A.H. El-Shazly, M.R. Elmarghany, M.N. Sabry, N. Nady, Effect of adding functionalized graphene on the performance of PVDF membrane in direct contact membrane distillation, Key Eng. Mater., 801 KEM (2019) 337–342.

[78] A. Dastbaz, J. Karimi-Sabet, H. Ahadi, Y. Amini, Preparation and characterization of novel modified PVDF-HFP/GO/ODS composite hollow fiber membrane for Caspian Seawater desalination, Desalination, 424 (2017) 62–73.

[79] Y. Li, L. Zhu, Evaluation of the antifouling and photocatalytic properties of novel poly(vinylidene fluoride) membranes with a reduced graphene oxide–Bi$_2$WO$_6$ active layer, J. Appl. Polym. Sci., 134 (2017) 1–7.

[80] D.H. Seo, S. Pineda, Y.C. Woo, M. Xie, A.T. Murdock, E.Y.M. Ang, Y. Jiao, M.J. Park, S. Il Lim, M. Lawn, F.F. Borghi, Z.J. Han, S. Gray, G. Millar, A. Du, H.K. Shon, T.Y. Ng, K. Ostrikov, Anti-fouling graphene-based membranes for effective water desalination, Nat. Commun., 9 (2018) 1–12.

[81] W. Intrchom, S. Roy, M.S. Humoud, S. Mitra, Immobilization of graphene oxide on the permeate side of a membrane distillation membrane to enhance flux, Membranes (Basel), 8 (2018) 21–23.

[82] J. Ren, J. Li, Z. Xu, Y. Liu, F. Cheng, Simultaneous anti-fouling and flux-enhanced membrane distillation via incorporating graphene oxide on PTFE membrane for coking wastewater treatment, Appl. Surf. Sci., 531 (2020) 147349, doi: 10.1016/j.apsusc.2020.147349.

[83] I. Gupta, J. Chakraborty, S. Roy, E.T. Farinas, S. Mitra, Nanocarbon immobilized membranes for generating bacteria and endotoxin free water via membrane distillation, Sep. Purif. Technol. 259 (2021) 118133. https://doi.org/10.1016/j.seppur.2020.118133.

[84] M. Wen, M. Chen, K. Chen, P.L. Li, C. Lv, X. Zhang, Y. Yao, W. Yang, G. Huang, G.K. Ren, S.J. Deng, Y.K. Liu, Z. Zheng, C.G. Xu, D.L. Luo, Superhydrophobic composite graphene oxide membrane coated with fluorinated silica nanoparticles for hydrogen isotopic water separation in membrane distillation, J. Membr. Sci., 626 (2021) 119136, doi: 10.1016/j.memsci.2021.119136.

[85] M. Wen, M. Chen, G.K. Ren, P.L. Li, C. Lv, Y. Yao, Y.K. Liu, S.J. Deng, Z. Zheng, C.G. Xu, D.L. Luo, Enhancing the selectivity of hydrogen isotopic water in membrane distillation by using

graphene oxide, J. Membr. Sci., 610 (2020) 118237, doi: 10.1016/j. memsci.2020.118237.

[86] Y. Mao, Q. Huang, B. Meng, K. Zhou, G. Liu, A. Gugliuzza, E. Drioli, W. Jin, Roughness-enhanced hydrophobic graphene oxide membrane for water desalination via membrane distillation, J. Membr. Sci., 611 (2020) 118364, doi: 10.1016/j. memsci.2020.118364.

[87] H. Qiu, Y. Peng, L. Ge, B. Villacorta Hernandez, Z. Zhu, Pore channel surface modification for enhancing anti-fouling membrane distillation, Appl. Surf. Sci., 443 (2018) 217–226.

[88] Q.W. Su, H. Lu, J.Y. Zhang, L.Z. Zhang, Fabrication and analysis of a highly hydrophobic and permeable block GO-PVP/PVDF membrane for membrane humidification-dehumidification desalination, J. Membr. Sci., 582 (2019) 367–380.

[89] L. Martínez-Díez, M.I. Vázquez-González, Temperature and concentration polarization in membrane distillation of aqueous salt solutions, J. Membr. Sci., 156 (1999) 265–273.

[90] A. Politano, P. Argurio, G. Di Profio, V. Sanna, A. Cupolillo, S. Chakraborty, H.A. Arafat, E. Curcio, Photothermal membrane distillation for seawater desalination, Adv. Mater., 29 (2017) 1–6.

[91] D. Jaque, L. Martínez Maestro, B. Del Rosal, P. Haro-Gonzalez, A. Benayas, J.L. Plaza, E. Martín Rodríguez, J. García Solé, Nanoparticles for photothermal therapies, Nanoscale, 6 (2014) 9494–9530.

[92] M. Gao, L. Zhu, C.K. Peh, G.W. Ho, Solar absorber material and system designs for photothermal water vaporization towards clean water and energy production, Energy Environ. Sci., 12 (2019) 841–864.

[93] Y. Lin, Z. Chen, L. Fang, M. Meng, Z. Liu, Y. Di, W. Cai, S. Huang, Z. Gan, Copper nanoparticles with near-unity, omnidirectional, and broadband optical absorption for highly efficient solar steam generation, Nanotechnology, 30 (2019) 015402.

[94] L. Huang, J. Pei, H. Jiang, X. Hu, Water desalination under one sun using graphene-based material modified PTFE membrane, Desalination, 442 (2018) 1–7.

[95] B. Hou, D. Kong, Z. Chen, Z. Shi, H. Cheng, D. Dong Guo, X. Wang, Flexible graphene oxide/mixed cellulose ester films for electricity generation and solar desalination, Appl. Therm. Eng., 163 (2019) 114322, doi: 10.1016/j. applthermaleng.2019.114322.

[96] L. Li, L. Zang, S. Zhang, T. Dou, X. Han, D. Zhao, Y. Zhang, L. Sun, Y. Zhang, GO/CNT-silica Janus nanofibrous membrane

for solar-driven interfacial steam generation and desalination, J. Taiwan Inst. Chem. Eng., 111 (2020) 191–197.

[97] X. Wu, T. Gao, C. Han, J. Xu, G. Owens, H. Xu, A photothermal reservoir for highly efficient solar steam generation without bulk water, Sci. Bull., 64 (2019) 1625–1633.

[98] L. Zhao, P. Wang, J. Tian, J. Wang, L. Li, L. Xu, Y. Wang, X. Fei, Y. Li, A novel composite hydrogel for solar evaporation enhancement at air-water interface, Sci. Total Environ., 668 (2019) 153–160.

[99] F. Tao, Y. Zhang, B. Wang, F. Zhang, X. Chang, R. Fan, L. Dong, Y. Yin, Graphite powder/semipermeable collodion membrane composite for water evaporation, Sol. Energy Mater. Sol. Cells, 180 (2018) 34–45.

[100] B. Hou, Z. Shi, D. Kong, Z. Chen, K. Yang, X. Ming, X. Wang, Scalable porous Al foil/reduced graphene oxide/Mn$_3$O$_4$ composites for efficient fresh water generation, Mater. Today Energy, 15 (2020) 100371, doi: 10.1016/j.mtener.2019.100371.

[101] M. Kim, K. Yang, Y.S. Kim, J.C. Won, P. Kang, Y.H. Kim, B.G. Kim, Laser-induced photothermal generation of flexible and salt-resistant monolithic bilayer membranes for efficient solar desalination, Carbon N. Y., 164 (2020) 349–356.

[102] X. Guo, H. Gao, S. Wang, L. Yin, Y. Dai, Scalable, flexible and reusable graphene oxide-functionalized electrospun nanofibrous membrane for solar photothermal desalination, Desalination, 488 (2020) 114535, doi: 10.1016/j. desal.2020.114535.

[103] L. Shi, Y. Wang, L. Zhang, P. Wang, Rational design of a bi-layered reduced graphene oxide film on polystyrene foam for solar-driven interfacial water evaporation, J. Mater. Chem. A, 5 (2017) 16212–16219.

[104] Y. Li, T. Gao, Z. Yang, C. Chen, Y. Kuang, J. Song, C. Jia, E.M. Hitz, B. Yang, L. Hu, Graphene oxide-based evaporator with one-dimensional water transport enabling high-efficiency solar desalination, Nano Energy, 41 (2017) 201–209.

[105] A. Guo, X. Ming, Y. Fu, G. Wang, X. Wang, Fiber-based, double-sided, reduced graphene oxide films for efficient solar vapor generation, ACS Appl. Mater. Interfaces, 9 (2017) 29958–29964.

[106] Y. Li, T. Gao, Z. Yang, C. Chen, W. Luo, J. Song, E. Hitz, C. Jia, Y. Zhou, B. Liu, B. Yang, L. Hu, 3D-printed, all-in-one evaporator for high-efficiency solar steam generation under 1 sun illumination, Adv. Mater., 29 (2017) 1–8.